Aalborg Universitet

An Intelligent Synchronous Power Control for Grid-Forming Inverters Based on Brain Emotional Learning

Oshnoei, Arman; Sorouri, Hoda; Teodorescu, Remus; Blaabjerg, Frede

An Intelligent Synchronous Power Control for Grid-Forming Inverters based on Brain Emotional Learning

Arman Oshnoei, *Member, IEEE*, Hoda Sorouri, Remus Teodorescu, *Fellow, IEEE*, and Frede Blaabjerg, *Fellow, IEEE*

Abstract—Grid-forming inverters (GFMI) are prone to have small-signal stability problems when connected to a stiff ac grid. Such stability problems originate significantly from the absence of GFMI control adaptivity to the varying short-circuit ratio (SCR). To confront this challenge, this letter proposes an intelligent synchronous power control (SPC) scheme that is robust against a wide range of SCR of the ac grid. The letter focuses on the design and digital implementation of brain emotional learning to provide adaptive tuning of the SPC control parameters, enabling the system to quickly adapt to changes in SCR. The approach passes the dependency of the active power control loop with the SPC on the operating point conditions, which enhances the system's robustness. Both theoretical and experimental validations confirmed the effectiveness of the proposed approach.

Index Terms—Artificial intelligence, stability, synchronous power controller, virtual inertia, grid forming inverters.

I. INTRODUCTION

GRid-forming inverters (GFMI) can regulate the grid voltage and frequency more effectively than synchronous machines when operating as voltage-controlled sources due to their fast response and enhanced controllability [1], [2]. The implementation of these functionalities heavily relies on effective power control. Various power control schemes have been suggested, among which the simplest one is the $P - \omega$ and $Q - V$ droop feature of the synchronous generator (SG) in both active power control loop (APCL) and reactive power control loop (RPCL). Although basic droop control does not inherently incorporate synthetic inertia emulation, modifications to this control method can overcome this limitation. As demonstrated in [3], when the APCL is equipped with a first-order low-pass filter, the basic droop control can be transformed into an equivalent of virtual SG (VSG) technology, enabling inertia emulation. The concept of VSG is proposed by mimicking the swing equation of an SG. According to the findings in [4], it is not crucial to reproduce the swing equation precisely as synchronous power controller (SPC)-based power control can flexibly realize the inertia emulation with inherent droop.

The VSG control structure is enhanced in the previous studies to achieve different control purposes. In [5], a power oscillation damper, which utilizes a band-pass filter-based supplementary controller, is incorporated into the standard VSG control to mitigate the power oscillations. A control strategy that links VSG and fractional-order control is proposed [6] in order to enhance power oscillations' damping. A fuzzy-based VSG is proposed in

[7] to improve the system frequency performance. However, the fuzzy rules considerably influence the controller's performance as they fully rely on the experience of the designer. One of the drawbacks of VSG control is that the adjustment of the parameters, such as damping ratio and closed-loop bandwidth, is restricted by the inertial constant and droop coefficient [8]. Thus, a VSG control developed for a high inertia condition in the standalone mode could lead to a significant overshoot and an extended settling time in step response in the grid-connected mode. Simultaneously achieving both control objectives defined in the grid-connected and standalone modes is not possible with a VSG control. Hence, in [9], the VSG control incorporates a zero to develop a lead-lag controller known as SPC. Consequently, the step response is independent of the inertial time constant and droop coefficient. A few studies have been conducted regarding the parameter design of the SPC. In [10], a pole/zero cancellation method assigns $P - \omega$ droop and initial constant individually. In [1], [8], [11], the closed-loop transfer function of the SPC loop is extracted, and a connection between design parameters (damping coefficient and inertia constant) and dynamic performance is established. However, the SPC techniques presented in these studies are developed based on a small signal model designed by linearizing the system at a given operating point. Therefore, in the case of unexpected changes in the GFMI's parameters (e.g., grid impedance variations), ensuring a favorable response is challenging, and GFMI may fail to reach a stable operating point during grid faults.

The main contribution of this letter is the design and verification of a real-time method to choose the SPC parameters automatically for any operating condition of a GFMI. To achieve this goal, the brain emotional learning (BEL) (a beneficial intelligent method in handling model complexity and uncertainty [13]) is used. During the design process, a small-signal analysis obtains appropriate initial adjustments for the SPC parameters. Subsequently, the parameters are modified in an online fashion using the proposed BEL intelligent method. Unlike the conventional SPC system commonly designed for a specified operating condition [1], [8]-[11], the proposed approach eliminates the reliance of the control system on the operating conditions, which improves the converter's robustness against grid impedance variations. Both theoretical and experimental validations confirmed the feasibility of the proposed approach.

II. SYSTEM DESCRIPTION

Fig. 1 (a) shows the test system in which a GFMI is connected to the grid at the point of common coupling (PCC) through a three-phase LC filter. C_f and L_f are the capacitance and inductance of the LC filter. A three-phase RL branch ($Z_g = r_g + j\omega l_g$) emulates the grid impedance. The implementation

of the GFMI comprises a voltage source inverter with the inner current and voltage regulation using PI controllers in *dq* frame. The DC source is assumed to be ideal, thereby decoupling the AC and DC sides. The control diagram of the SPC is depicted in Fig. 1 (b). In contrast to the VSG controller, the SPC offers a supplementary degree of freedom to the system without any increase in the system order, giving a natural $P-\omega$ droop feature that can be configured independently of the damping and inertia parameters. The transfer function for the SPC is presented below

$$K_{SPC}(s) = \frac{k_p s + k_i}{s + k_g} \quad (1)$$

The controller gains in the equation, namely k_p, k_i, and k_g, are used to tune the system's behavior, with k_g being utilized to configure the system's $P-\omega$ droop characteristic. From Fig. 1 (b), the closed-loop transfer function ($G_{cl}(s)$) is derived as follows:

$$G_{cl}(s) = \frac{P_g}{P_{in}} = \frac{\frac{v_o v_g}{X_g}(k_p s + k_i)}{s^2 + (k_p \frac{v_o v_g}{X_g} + k_g)s + k_i \frac{v_o v_g}{X_g}} \quad (2)$$

where P_g and P_{in} are the active power and its set-point value; v_g and v_o are the RMS values of the grid and capacitance voltages, respectively; and $X_g = \omega l_g$ is the grid reactance. Eq. (2) can be expressed as a generalized second-order equation as below

$$G_{cl}(s) = \frac{(2\zeta\omega_n - k_g)s + \omega_n^2}{s^2 + 2\zeta\omega_n s + \omega_n^2} \quad (3)$$

where $\zeta = \frac{\frac{v_o v_g}{X_g} k_p + k_g}{2\omega_n}$ and $\omega_n = \sqrt{\frac{v_o v_g}{X_g} k_i}$. The $P-\omega$ response can be described by

$$\frac{P_g(s)}{\omega_g(s)} = \frac{-\frac{v_o v_g}{X_g}(s + k_g)}{s^2 + 2\zeta\omega_n s + \omega_n^2} \quad (4)$$

where ω_g is the nominal angular speed of the grid. Additionally, the $P-f$ droop slope is determined by the steady-state value of Eq. (4), and it can be described as

$$D_p = \frac{2\pi k_g}{S_r k_i} \quad (5)$$

where S_r is the inverter rating.

According to the droop characteristic, the system's angular frequency should be maintained within the permissible interval of $[\omega_{min}, \omega_{max}]$. As such, the $P-\omega$ droop coefficient in (5) must comply with the saturation boundaries defined in the following.

$$0 \leq D_p \leq \frac{P_{max} - P_{in}}{\omega_{max} - \omega_{min}} \quad (6)$$

where $P_{max} = \sqrt{S_r^2 - Q_{in}^2}$; P_{max} is the maximum active power and Q_{in} is the reactive power reference. The virtual inertia J is also needed to have upper and lower boundaries to avoid long-term overcapacity of inverter ($J_{min} \leq J \leq J_{max}$) [12]. The maximum value of virtual inertia J_{max} is associated with the instantaneous power capacity constraints of the inverter, and the minimum virtual inertia J_{min} is needed to meet the minimum frequency stability provision. Accordingly, the upper and the lower limits of virtual inertia can be developed as

$$PO(J_{max})\Delta\omega_{max} \leq P_{max} - P_{in}$$

$$J_{min} > \frac{\Delta P_d}{|d\omega/dt|_{max}} \quad (7)$$

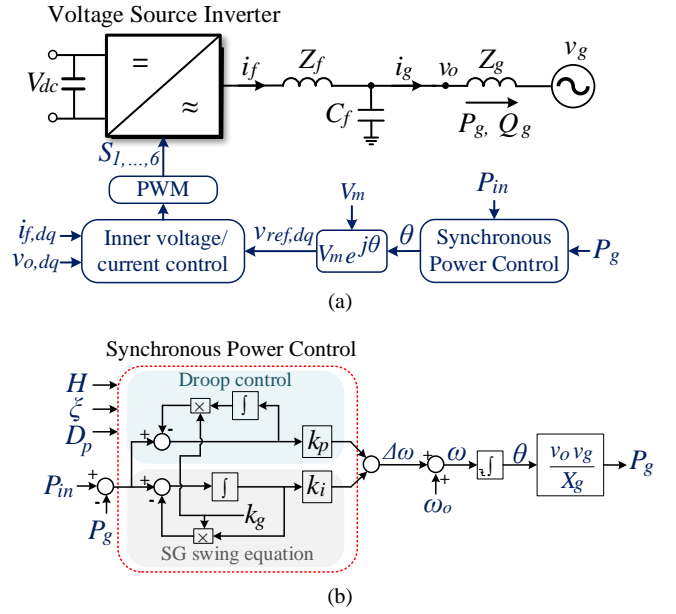Voltage Source Inverter

(a)

(b)

Fig. 1. Schematic of the proposed GFMI setup. (a) topology; (b) control strategy.

where $PO(J_{max})$ represents the VSG output power overshoot with J_{max} caused by a step disturbance in frequency. P_{max} represents the instantaneous power capacity limitation of the inverter, ΔP_d represents the output power change due to disturbance, and $|d\omega/dt|_{max}$ is the required maximum frequency change according to the grid code. Using (8), the moment of inertia can be converted to H, representing the time required to accelerate the rotational speed from zero to ω_n.

$$H = \frac{J\omega_n^2}{2S_r} \quad (8)$$

Using (7) and (8), the upper and lower constraints for H can be set.

III. PROPOSED SPC DESIGN STRATEGY

This section presents the use of the proposed BEL to regulate the control parameters optimally. In the regulation process, a performance analysis is conducted to determine an initial adjustment for the gains. Subsequently, the BEL method is intended to provide accurate online adaptation of the control gains.

A. Gains Design Based on Performance Analysis: Stage 1

The integral gain k_i can be adjusted in terms of suitable inertia needed for the system as [1]:

$$k_i = \frac{\omega_g}{2HS_r} \quad (9)$$

where H is inertia constant. After determining k_i through the criterion given in equation (9), the droop slope can be exclusively defined by the value of k_g. Then, the criterion to set k_g and the proportional gain k_p can be described as follows

$$k_g = \frac{D_p}{2H}, \quad k_p = 2\zeta\sqrt{\frac{\omega_g}{2HS_r \frac{v_o v_g}{X_g}}} - \frac{D_p}{2H \frac{v_o v_g}{X_g}} \quad (10)$$

TABLE I
PARAMETERS OF THE GFMI SETUP

| Parameters	Description	Value
v_g	Grid voltage (RMS)	70 V
ω_g	Grid's nominal angular speed	100π rad/s
ω_0	Nominal frequency	100π rad/s
l_g and r_g	Line impedance	5.4 mH and 0.2 Ω
L_f and C_f	LC-filter	2.4 mH and 15 μF
S_r	Inverter rating	1 kW
V_{dc}	DC-side voltage	200 V
k_{pv}, k_{iv}	Voltage controller	1, 50
k_{pc}, k_{ic}	Current controller	0.0729, 0.0047
λ_1, λ_2	Weighting coefficients (SI)	1.58, 1.12
$\delta_1, \delta_2, \delta_3$	Weighting coefficients (ES)	0.92, 1.40, 1.33
k_{po}, k_{io}, k_{go}	SPC controller	0.0157, 0.0026, 0.5
SF_1, SF_2, SF_3	Scaling factors	0.96, 0.8, 1.1
f_{sw}	Switching frequency	20 kHz
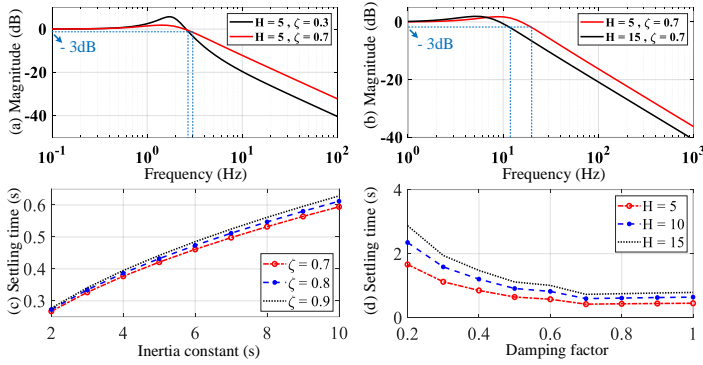
Fig. 2. Performance analysis of (3): (a), (b) closed-loop magnitude-frequency characteristics; (c) closed-loop step response settling time when H changes from 2 to 10; (d) closed-loop step response settling time when ζ changes from 0.2 to 1.

The constraints defined in (6) and (7) directly influence the upper and lower boundaries for control parameters K_p, K_i, and K_g. The system parameters are provided in Table I. In this study, D_p is chosen as 10 kW/Hz. The closed-loop magnitude–frequency characteristics are shown in Figs. 2 (a)-(b) to evaluate the system's performance based on the SPC controller. Fig. 2 (a) shows that the SPC-based system has larger bandwidth under a suitable damping factor ($\zeta = 0.7$). Fig. 2 (b) indicates that the system's bandwidth is decreased when the inertia constant (H) changes from 5 to 15 s. From Fig. 2 (c), the settling time is impacted by an increasing H. It is seen from Fig. 2 (d) that in the value range $\zeta = [0.7\ 1]$, the settling time does not vary relatively. Hence, ζ, has been chosen as 0.7 to ensure that the overshoot and settling time of the step response fall within acceptable limits. The selection of H can be determined based on the inertia constant of the SG within the range of 0-10 seconds while keeping the same power level.

B. Supplementary Gains Design Based on Proposed BEL Approach: Stage 2

This approach consists of several components, namely the Amygdala (A) (responsible for emotional learning), the Orbitofrontal cortex (O), the sensory cortex, and the Thalamus [13]. The model has two inputs: the sensory input (SI) and the emotional signal (ES). With zero initial conditions, the BEL output u is given as

$$u(t) = SI(t)[\alpha \int_0^t SI(t)[max(0, ES(t) - A(t))]dt$$
$$- \beta \int_0^t SI(t)[A(t) - O(t) - ES(t)]dt] \quad (11)$$

Remark I. *Theorem 1 given in [13] is used to identify the convergence conditions for choosing α and β (α and β are the learning and inhibition rates, respectively). The response speed relies on α and β. α ideally should be slightly higher than β for the output to follow the references (which are P_{in}^* and ω_0) closely. Here, α and β are chosen as 0.86 and 0.98, respectively, to reach a moderately damped response.*

Besides, in order to attain the favorable performance of the BEL, constituting an empirical relation between SI, ES, and output $u = [k_i, k_g, k_p]$ is essential. The SI and ES inputs for BEL are selected as (12) and (13), respectively.

$$SI = \lambda_1(P_{in}^* - P_g) + \lambda_2 \int (P_{in}^* - P_g)dt \quad (12)$$

$$ES = \delta_1(\omega_0 - \omega) + \delta_2 \int (\omega_0 - \omega)dt + \delta_3 u \quad (13)$$

where λ_1 and λ_2 are weighting coefficients for the SI function; δ_1, δ_2, and δ_3 denote weighting coefficients for the ES function.

The SI and ES functions aim to ensure a fast response, minimize overshoot and steady-state error, and minimize deviation from a chosen reference. Therefore, SI is chosen as the output of a PI block in response to the difference between the reference active power P_{in}^* and the generated power P_g (Eq. (12)). Similarly, ES is chosen as the output of a PI block responding to the difference between the reference grid frequency ω_0 and the actual grid frequency ω (Eq. (13)).

The control command u is preserved within the following saturation bounds.

$$u_{min} \leq (\alpha + \beta)(\lambda_1 + \lambda_2)^2(\delta_1 + \delta_2)y^3 dt \leq u_{max} \quad (14)$$

where u_{min} and u_{max} are the BEL output's minimum and maximum values.

Fig. 3 shows the proposed BEL framework for designing SPC parameters. The BEL output also considers desirable scaling factors (SF) to achieve optimal results. A particle swarm optimization algorithm is used for optimizaing the SFs and weighting coefficients through minimizing an objective function which is the integral of time multiplied by the square of the active power and frequency errors. The notations k_{io}, k_{po}, and k_{go} are the initial settings of the controller, which are obtained in stage 1 (section III.A).

Remark II. *The BEL is a model-free intelligent method with a simplistic control framework, making it viable for practical applications in real-time. This method has a reinforcement learning process as a principle, effectively tackling disturbances and uncertainties in the system. The common features of this method and the main reasons for its selection are twofold. First, this method has the capability to produce dynamic outputs for control purposes. This comprises updating the SPC tuning coefficients (gains) concerning the operating point deviations and the existence of any disturbance. Second, this intelligent technique has model-free configurations, and their functionalities are not affected by the GFMI's complexities. This feature*
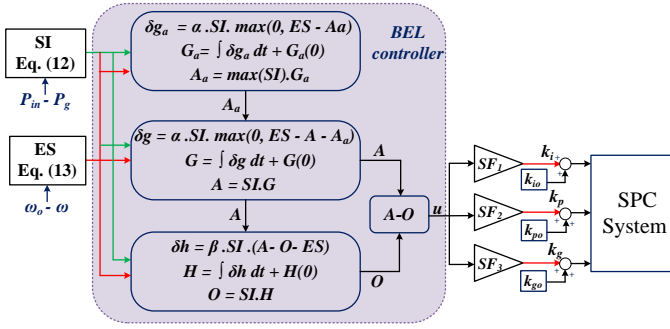
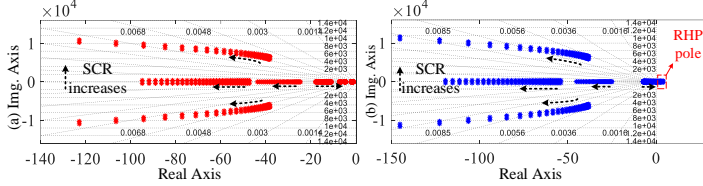Fig. 3. The framework of the proposed BEL-based tuning scheme.

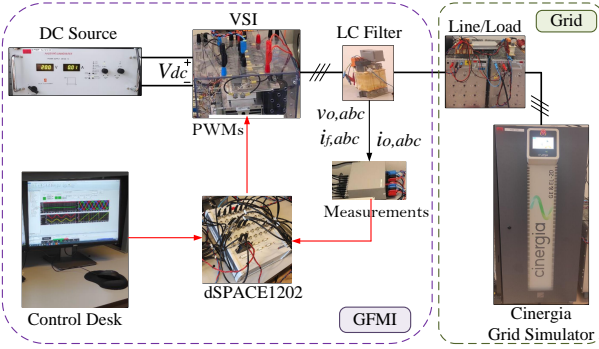Fig. 4. Dominant eigenvalues of overall GFMI with (a) proposed BEL-SPC; (b) conventional SPC.

Fig. 5. View of the experimental setup.

allows for more flexibility in design and enables its use in practice. The application of this method in this letter is based on the supervisory (online) regulation application.

IV. STABILITY INVESTIGATION

This section aims to evaluate the stability of the whole system and its robustness against the SCR variations, where state-space models of the physical circuit, the inner current and voltage control loops, and the APCL and RPCL loops are extracted based on the small-signal models. The dominant eigenvalues of the system with and without the proposed method under different SCR conditions (a sweep of SCR from 4.3 to 40) are shown in Fig. 4. As observed, by using the conventional SPC, the system falls into an instability region for SCR > 12.31. This implies that the SPC design procedure presented in Section III.A (stage 1) becomes invalid in the case of grid inductance variations. In contrast, the BEL determines in real-time the proper control parameters (k_i, k_p, k_g) for each operating point. In this case, the eigenvalues remain inside the left half plane, irrespective of grid inductance wide deviations, indicating that the GFMI robustness is significantly enhanced thanks to the BEL method.
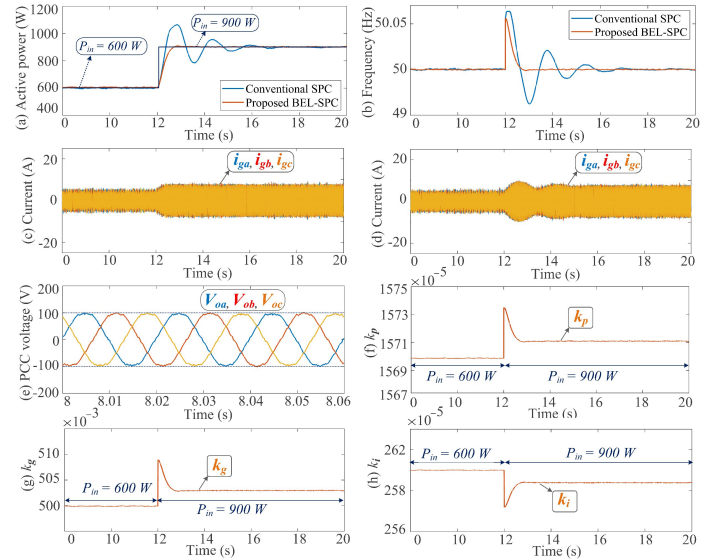

Fig. 6. Experimental tests for a step change in P_{in} when SCR=8.66; (a) active power, (b) frequency deviation; (c) current (proposed BEL-SPC), (d) current (conventional SPC), (e) PCC volatge (proposed BEL-SPC), (f), (g), (h) variations of the control parameters (k_p, k_g, k_i).
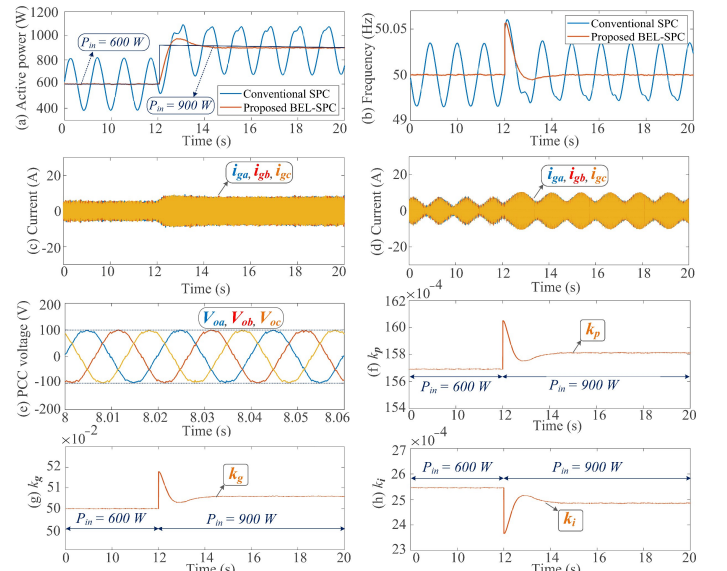

Fig. 7. Experimental tests for a step change in P_{in} when SCR=13; (a) active power, (b) frequency deviation; (c) current (proposed BEL-SPC), (d) current (conventional SPC), (e) PCC volatge (proposed BEL-SPC), (f), (g), (h) variations of the control parameters (k_p, k_g, k_i).

V. EXPERIMENTAL RESULTS

The proposed method is verified using a GFMI laboratory setup executed based on the schematic depicted in Fig. 1. Fig. 5 shows the experimental setup. The power grid is emulated by a Cinergia Grid Simulator. A ds1202 dSPACE system executes both algorithms of the BEL intelligent method and the GFMI control system. Fig. 6 (a)-(d) shows the experimental comparisons (P_g, ω, $i_{g,abc}$) when P_{in} steps from $600W$ to $900W$ in a stiff-grid connection (SCR = 8.66, estimated by grid inductance Lg). As it can be seen, the proposed BEL-SPC control offers better oscillation damping, faster and smoother dynamics, and a lower peak in active power and frequency changes in comparison with conventional SPC control. The PCC

voltage ($V_{o,abc}$) with the proposed method is plotted in Fig. 6 (e). As seen, the proposed BEL-SPC control complies with the limitations of the IEEE Standard 519-2014 regarding total harmonic distortion. The generated control parameters by BEL-based approach under the applied active power change are shown in Fig. 6 (g)-(h). The figure illustrates that the BEL can adapt its output dynamically, ensuring proper regulation of P_g at the reference value while minimizing fluctuations. Fig. 7 compares the system's performance with SCR=13. It can be observed that when using the conventional SPC, the system becomes unstable as the Lg is reduced. In contrast, the proposed control scheme offers a satisfactory performance even with a reduced Lg, demonstrating the method's robustness against changes in grid inductance. The experimental results verify the stability analysis carried out in section IV.

VI. CONCLUSION

This letter proposes an intelligent SPC scheme designed for a GFMI that has been demonstrated to be robust within a wide range of SCRs. The purpose was to track a desired active power independently of the operating point. The determination of SPC parameters conventionally relies on heuristic methods, which require simulation or experimental results for each specific point and can be a time-consuming process, resulting in a challenging problem. In contrast, the proposed BEL method offers an automated approach by adjusting the control parameters to any operating condition. The effectiveness of the proposed control scheme is verified through analytical and experimental studies in two different cases, demonstrating the system's ability to remain stable despite significant variations in grid inductance.

REFERENCES

[1] R. L. de Araujo Ribeiroet al., "Adaptive Grid Impedance Shaping Approach Applied for Grid-Forming Power Converters," *IEEE Access*, vol. 10, pp. 83096–83110, Aug. 2022.

[2] R. Heydari et al., "Model-Free Predictive Control of Grid-Forming Inverters With LCL Filters," *IEEE Trans. Power Electron.*, vol. 37, no. 8, pp. 9200–9211, Aug. 2022.

[3] D. Pan et al., "Transient Stability of Voltage-Source Converters With Grid-Forming Control: A Design-Oriented Study," *IEEE Journal of Emerging and Selected Topics in Power Electronics*, vol. 8, no. 2, pp. 1019–1033, June 2020.

[4] L. Harnefors et al., "Robust analytic design of power-synchronization control," *IEEE Trans. Ind. Electron.*, vol. 66, no. 8, pp. 5810–5819, Aug. 2019.

[5] G. N. Baltas et al., "Grid forming power converters tuned through artificial intelligence to damp subsynchronous interactions in electrical grids," *IEEE Access*, vol. 8, pp. 93369–93379, 2020.

[6] Y. Yu et al., "Fractional-Order Virtual Synchronous Generator," in *IEEE Trans. Power Electron.*, vol. 38, no. 6, pp. 6874–6879, June 2023.

[7] A. Karimi et al., "Inertia response improvement in AC microgrids: A fuzzy-based virtual synchronous generator control," *IEEE Trans. Power Electron.*, vol. 35, no. 4, pp. 4321–4331, Apr. 2020.

[8] X. Meng et al., "A generalized droop control for gridsupporting inverter based on comparison between traditional droop control and virtual synchronous generator control," *IEEE Trans. Power Electron.*, vol. 34, no. 6, pp. 5416–5438, Jun. 2019.

[9] W. Zhang et al., "Synchronous power controller with flexible droop characteristics for renewable power generation systems," *IEEE Trans. Sust. Energy*, vol. 7, no. 4, pp. 1572–1582, Oct. 2016.

[10] X. Quan et al., "A novel order reduced synchronous power control for grid-forming inverters," *IEEE Trans. Ind. Electron.*, vol. 67, no. 12, pp. 10 989–10 995, Dec. 2020.

[11] W. Zhang et al., "Frequency support properties of the synchronous power control for grid-connected converters," *IEEE Trans. Ind. Appl.*, vol. 55, no. 5, pp. 5178–5189, Sep. 2019.

[12] X. Hou, Y. Sun, X. Zhang, J. Lu, P. Wang and J. M. Guerrero, "Improvement of Frequency Regulation in VSG-Based AC Microgrid Via Adaptive Virtual Inertia," in IEEE Transactions on Power Electronics, vol. 35, no. 2, pp. 1589–1602, Feb. 2020, doi: 10.1109/TPEL.2019.2923734.

[13] M. S. O. Yeganeh et al., "Intelligent Secondary Control of Islanded AC Microgrids: A Brain Emotional Learning-Based Approach," *IEEE Trans. Ind. Electron.*, vol. 70, no. 7, pp. 6711–6723, July 2023.